Stem Cell Reports
Article
ISSCR
OPEN ACCESS

Reduced PHOX2B stability causes axonal growth impairment in motor neurons with *TARDBP* mutations

Shio Mitsuzawa,[1,12] Naoki Suzuki,[1] Tetsuya Akiyama,[1] Mitsuru Ishikawa,[2] Takefumi Sone,[2] Jiro Kawada,[3,4] Ryo Funayama,[5] Matsuyuki Shirota,[6] Hiroaki Mitsuhashi,[7] Satoru Morimoto,[2] Kensuke Ikeda,[1] Tomomi Shijo,[1] Akiyuki Ohno,[1] Naoko Nakamura,[1] Hiroya Ono,[1] Risako Ono,[1] Shion Osana,[8] Tadashi Nakagawa,[5,9] Ayumi Nishiyama,[1] Rumiko Izumi,[1] Shohei Kaneda,[4,10] Yoshiho Ikeuchi,[4,11] Keiko Nakayama,[5] Teruo Fujii,[4] Hitoshi Warita,[1] Hideyuki Okano,[2] and Masashi Aoki[1,*]

[1]Department of Neurology, Tohoku University Graduate School of Medicine, 1-1 Seiryo-machi, Aoba-ku, Sendai 980-8574, Japan
[2]Department of Physiology, Keio University School of Medicine, 35 Shinanomachi, Shinjuku-ku, Tokyo 160-8582, Japan
[3]Jiksak Bioengineering Inc. 7-7 Shinkawasaki, Saiwai-ku, Kawasaki 212-0032, Japan
[4]Institute of Industrial Science, the University of Tokyo, 4-6-1 Komaba, Meguro-ku, Tokyo 153-8505, Japan
[5]Division of Cell Proliferation, United Centers for Advanced Research and Translational Medicine, Tohoku University Graduate School of Medicine, 2-1 Seiryo-machi, Aoba-ku, Sendai 980-8575, Japan
[6]Division of Interdisciplinary Medical Science, United Centers for Advanced Research and Translational Medicine, Tohoku University Graduate School of Medicine, 2-1 Seiryo-machi, Aoba-ku, Sendai 980-8575, Japan
[7]Department of Applied Biochemistry, School of Engineering, Tokai University, 4-1-1 Kitakaname, Hiratsuka, Kanagawa 259-1292, Japan
[8]Division of Biomedical Engineering for Health and Welfare, Graduate School of Biomedical Engineering, Tohoku University, 2-1 Seiryo-machi, Aoba-ku, Sendai 980-8575, Japan
[9]Department of Clinical Pharmacology, Faculty of Pharmaceutical Sciences, Sanyo-Onoda City University, 1-1-1 Daigaku-Doori, Sanyo-Onoda, Yamaguchi 756-0884, Japan
[10]Department of Mechanical Systems Engineering, Faculty of Engineering, Kogakuin University, 1-24-2 Nishishinjuku, Shinjuku-ku, Tokyo, 163-8677, Japan
[11]Institute for AI and Beyond, The University of Tokyo, 7-3-1 Hongo, Bunkyo-ku, Tokyo 113-0033, Japan
[12]Present address: Department of Neurology, Shodo-kai Southern Tohoku General Hospital, 1-2-5, Satonomori, Iwanuma, Miyagi 989-2483, Japan
*Correspondence: aokim@med.tohoku.ac.jp
https://doi.org/10.1016/j.stemcr.2021.04.021

SUMMARY

Amyotrophic lateral sclerosis (ALS) is an adult-onset incurable motor neuron (MN) disease. The reasons for selective MN vulnerability in ALS are unknown. Axonal pathology is among the earliest signs of ALS. We searched for novel modulatory genes in human MN axon shortening affected by *TARDBP* mutations. In transcriptome analysis of RNA present in the axon compartment of human-derived induced pluripotent stem cell (iPSC)-derived MNs, *PHOX2B* (paired-like homeobox protein 2B) showed lower expression in *TARDBP* mutant axons, which was consistent with axon qPCR and *in situ* hybridization. *PHOX2B* mRNA stability was reduced in *TARDBP* mutant MNs. Furthermore, *PHOX2B* knockdown reduced neurite length in human MNs. Finally, *phox2b* knockdown in zebrafish induced short spinal axons and impaired escape response. *PHOX2B* is known to be highly express in other types of neurons maintained after ALS progression. Collectively, *TARDBP* mutations induced loss of axonal resilience, which is an important ALS-related phenotype mediated by *PHOX2B* downregulation.

INTRODUCTION

Amyotrophic lateral sclerosis (ALS) is an incurable, progressive, adult-onset neurodegenerative disease, in which cortical, brainstem, and spinal motor neurons (MNs) are slowly destroyed, resulting in muscle weakness, atrophy, and finally death due to respiratory and swallowing dysfunction (Wijesekera and Leigh, 2009). The development of effective treatments has been hindered by a poor understanding of disease pathogenesis. The reasons for selective MN vulnerability in ALS are unknown.

Most cases of ALS are sporadic; whereas, about 10% of ALS patients have a family history (Taylor et al., 2016). Mutations of the *TARDBP* gene, encoding transactive response DNA binding protein 43 kDa (TDP-43), are found in 3% of familial ALS and 1.5% of sporadic ALS cases. Among Japanese familial ALS patients, *TARDBP* mutations are the third most common after *SOD1* (Cu/Zn superoxide dismutase) and *FUS* (fused in sarcoma) mutations (Nishiyama et al., 2017). Moreover, TDP-43 aggregates within spinal anterior horn neurons are observed in the majority of sporadic ALS patients (Mackenzie et al., 2007), suggesting a major contribution of TDP-43 to ALS pathogenesis.

TDP-43 is an RNA-binding protein of the heterogeneous nuclear ribonucleoprotein (hnRNP) family expressed mainly in the nucleus and partially in the cytoplasm, where it regulates RNA stability and translation (Buratti and Baralle, 2001; Coyne et al., 2014; Strong et al., 2007). In ALS with *TARDBP* mutations, mutant TDP-43 has been reported to cause abnormalities in various RNA metabolic functions such as splicing, stability, and transport (Kapeli et al., 2017). These processes are particularly critical for projection neurons such as MNs because the distal axon and synapses may be up to 1 m or more from the somas. The mechanisms contributing to the resilience of these structures throughout life have not been fully elucidated. In the *SOD1* mutant

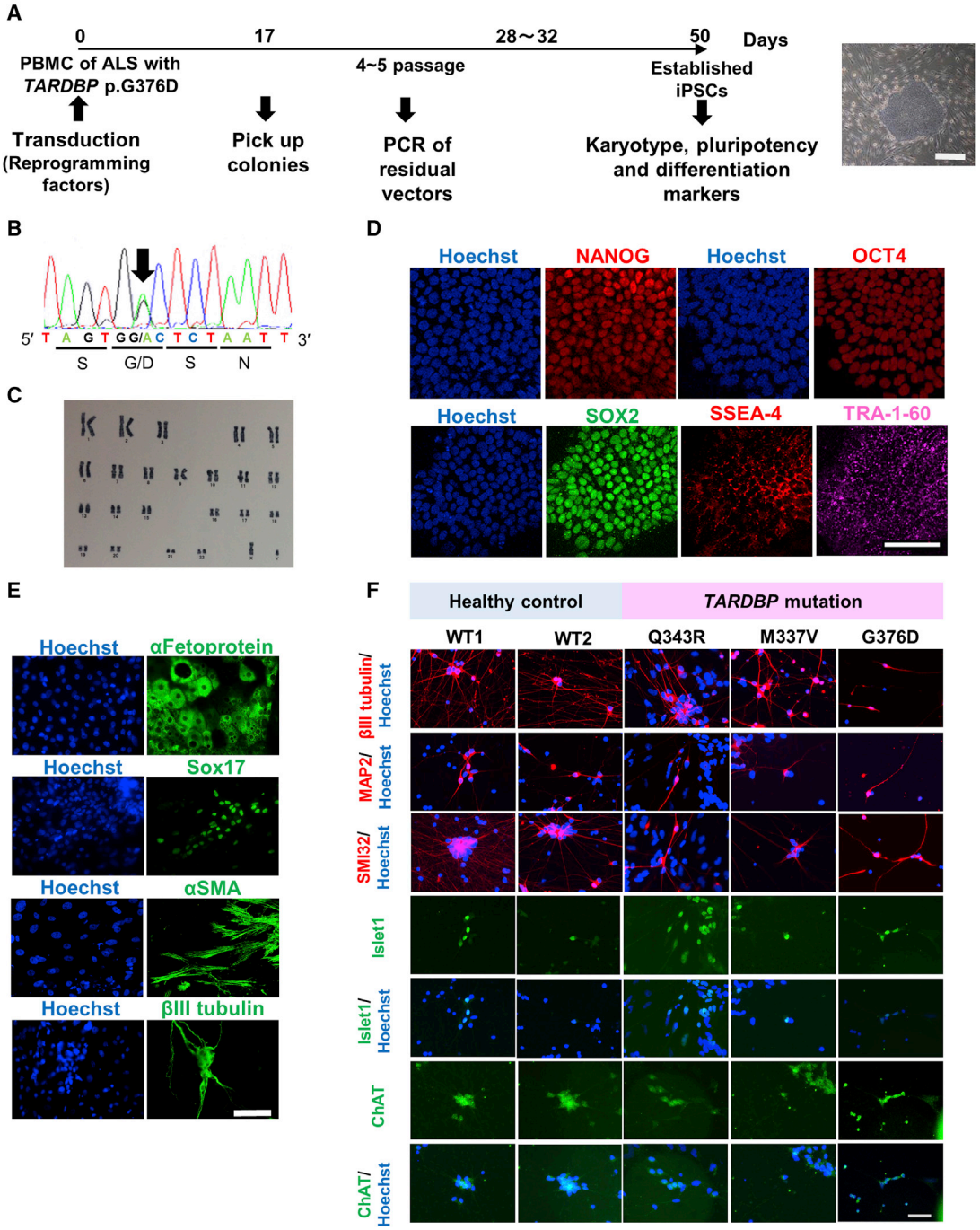

Figure 1. Phenotype evaluations of newly established iPSCs and iPSC-derived MNs

(A) Protocol for establishing iPSCs from the peripheral blood mononuclear cells (PBMCs) of a familial ALS patient harboring the *TARDBP* p.G376D mutation. The panel shows the selected colony. Scale bar, 500 μm.

(B) Reprogrammed PBMCs that formed colonies carried the same *TARDBP* p.G376D mutation as the familial ALS patient. The panel shows the heterozygous c.1127G > A change (black arrow) revealed by Sanger sequencing.

(C) Karyotype analysis of iPSCs harboring *TARDBP* p.G376D. No karyotype abnormality was detected.

(D) The established iPSCs expressed pluripotency markers as evidenced by immunocytochemistry. Scale bar, 100 μm.

(legend continued on next page)

mouse model of ALS, structural abnormalities in the axon have been reported to precede MN death (Tian et al., 2016). Moreover, MNs differentiated from ALS patient-derived induced pluripotent stem cells (iPSCs) with *TARDBP* mutations had shorter axons than healthy control MNs (Egawa et al., 2012; Fujimori et al., 2018). On the basis of these findings, we speculated that *TARDBP* mutations reduce the capacity to bind and stabilize mRNAs involved in axon homeostasis, resulting in functional and structural axonal abnormalities and ensuing neurodegeneration.

In this study, a transcription factor, *PHOX2B*, was identified by RNA sequencing (RNA-seq) analysis to be downregulated in iPSC-derived MN axons. The knockdown (KD) of *PHOX2B* shortened the neurite length of MNs compared with the control, consistent with an iPSC-derived MN phenotype in ALS patients with *TARDBP* mutations. In zebrafish, the KD of endogenous *phox2b* also reduced MN axon length and increased axon branching. These results indicated that reduced expression of *PHOX2B* may be associated with MN degeneration in ALS pathology.

RESULTS

Generation and phenotyping of MNs from iPSCs

iPSCs harboring the *TARDBP* p.G376D mutation were established from a 36-year-old male familial ALS patient with progressive muscle weakness of the upper extremities and head drop who died 1 year from onset (Mitsuzawa et al., 2018; Nishiyama et al., 2017). The iPSCs were validated by Sanger sequencing, karyotyping (normal), detection of pluripotency markers by immunocytochemistry, and three germ layer differentiation potential (Figures 1A–1E and S1A). All iPSCs used in this study (healthy control- and ALS-derived) were differentiated into MNs exhibiting a transitional embryonic body-like state, as described previously (Fujimori et al., 2018; Fujimori et al., 2017). Phenotype was confirmed by immunocytochemistry for the neuron-specific markers βIII tubulin, SMI32, and microtubule-associated protein 2 (MAP2), and for the MN-specific markers choline acetyltransferase (ChAT) and Islet1 (Figure 1F). The iPSCs used in this study are listed in Table S1.

TARDBP mutations reduce neurite length in iPSC-derived MNs

It has been reported that iPSC-derived MNs harboring *TARDBP* mutations (such as p.M337V) from ALS patients have shorter neurites than MNs derived from the iPSCs of healthy controls (Egawa et al., 2012; Fujimori et al., 2018). In this study, neurite length was measured by fluorescent signals that originate from the edge of MN precursor mass to the neurite ends upon transfection with an *EF-1α::Venus*, *HB9::Venus*, or *HB9::RFP* (red fluorescent protein) lentivirus vector. During culture, the average neurite length of *TARDBP* mutant MNs was significantly shorter than that of healthy control MNs by 33 days after differentiation (14 days post plating [dpp]) and remained shorter at the measurement endpoint when the neurites reached the well wall 17–21 dpp (Figures 2A and 2B).

Identification of genes associated with *TARDBP* mutation-induced axonal pathogenesis by RNA-seq

To identify molecules potentially related to *TARDBP* mutation-induced axonal pathology, we first conducted RNA-seq analysis using the axonal fractions of iPSC-derived MNs (Figure 3A). Candidate genes were identified based on the selection criteria outlined in the experimental procedures (Figures 3B; Tables S4, S5, S6, and S7). Enrichment analysis revealed that the transcripts of 252 genes associated with chloride transmembrane transport, MAPK cascade, and cell or neuron fate commitment were all significantly upregulated in axons derived from the iPSCs with a *TARDBP* mutation. In contrast, the transcripts of 220 genes associated with memory, cell motility, postsynaptic membrane potential, and axon or actin-related functions were significantly downregulated (Figure 3C). Enrichment analysis revealed that 16 of the downregulated transcripts were associated with significant changes in the neuronal soma, while 150 transcripts, 103 upregulated and 47 downregulated, were associated with the axon. We then focused on gene ontology (GO) categories, including terms like nerves, axons, transport, cytoskeleton, and inflammation. We also focused on those including the TDP-43 binding sequence UGUGUG (Tollervey et al., 2011) within the coding sequences or the 3′ untranslated regions (UTR) by RBP map (http://rbpmap.technion.ac.il). These strategies facilitated the identification of 61 candidate genes associated with *TARDBP* mutation-induced axonal pathology. Among these, we focused on *PHOX2B*, previously identified as essential for forming the neural crest and inducing MN differentiation (Nagashimada et al., 2012; Pattyn et al., 1999). Moreover, it was reported that *NEFL* mRNA was decreased and apoptosis increased in *PHOX2B* KD cells (Huber et al., 2005), suggesting that

(E) Demonstration of the three germ layer differentiation capacity of iPSCs by immunocytochemistry. The endodermal markers α-fetoprotein and SOX17, the mesodermal marker αSMA, and the ectodermal marker βIII tubulin, were all expressed by iPSCs maintained in a basic fibroblast growth factor-free medium. Scale bar, 100 μm. See also Figure S1A.

(F) Established iPSCs differentiated into MNs as verified by the expression of neuron-specific markers βIII tubulin, MAP2, and SMI32, and MN-specific markers Islet1 and ChAT. Scale bar, 50 μm. See also Tables S1 and S3.

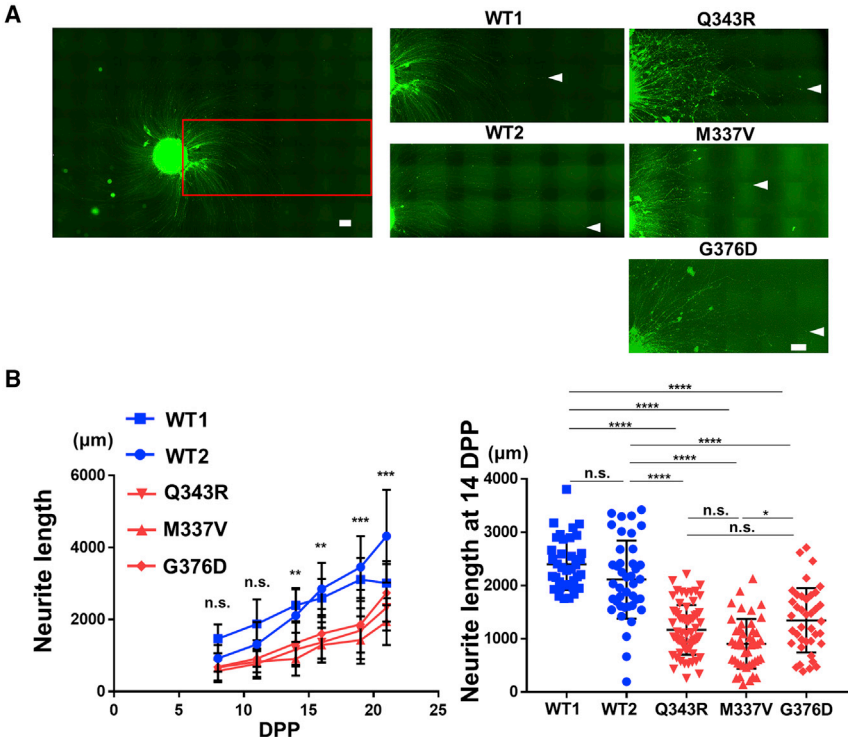

Figure 2. MNs derived from iPSCs harboring *TARDBP* mutations exhibited shorter neurites than did MNs derived for WT iPSCs

(A) Neurite lengths of iPSC-derived *TARDBP* mutant MNs were compared with those of healthy control MNs during culture. MNs were infected with *EF-1α::Venus* lentivirus vector, formed spheres, and then examined periodically under fluorescence microscopy. The white arrowheads indicate the most distal end of each neurite. Neurite lengths were compared among two healthy control MN populations derived from two separate iPSC lines (WT1 and WT2) (left) and *TARDBP* mutants (Q343R, M337V, and G376D) (right). Scale bar, 300 μm.

(B) Changes in MN neurite length over time. Twenty to 74 neurites were analyzed per group for one experiment, depending on the time post differentiation. A comparison between the healthy control and *TARDBP* mutant groups showed that the neurite length significantly decreased in the *TARDBP* mutant group from day 14 (left graph). Statistical comparison at 14 dpp among cell lines also confirmed that *TARDBP* mutant MNs had significantly shorter neurites than had healthy control MNs (right graph). Repeated measures ANOVA with post hoc Tukey HSD tests for comparison between healthy control and *TARDBP* mutant groups. Two-way ANOVA with post hoc Tukey HSD tests for among each cell lines. **p < 0.01, ****p < 0.0001

PHOX2B is related to MN vulnerability and axonal morphology. Furthermore, *PHOX2A*, a paralogous gene product of *PHOX2B* in structure, was reported to form heterodimers with PHOX2B *in vitro* (Di Lascio et al., 2016) and was also among the 61 differentially expressed genes from RNA-seq axon fraction.

PHOX2B mRNA has TDP-43 binding consensus sequence in 3′ UTR (NCBI Reference Sequence: NM_003924.4) and its expression was reduced in *TARDBP* mutant axons with RNA-seq and qPCR (Figures 3D and S1B for qPCR results of *TARDBP* p.N345K [N345K] [Leventoux et al., 2020]), it was selected for further investigation. PHOX2B protein expression was significantly reduced in *TARDBP* mutant MNs compared with that in MNs derived from healthy controls (Figure 3E).

Confirmation of reduced *PHOX2B* expression using isogenic *TARDBP*-mutated iPSCs

To confirm the specificity of *PHOX2B* downregulation by ALS-causative *TARDBP* mutations, we examined expression changes in wild-type 1 (WT1) (CiRA 201B7)-derived isogenic lines harboring these mutations. Heterozygous and homozygous mutations of p.M337V and p.G298S were generated in iPSCs, and pluripotency was verified by selective marker expression (Figure S2A). Furthermore, MN phenotype was verified by selective marker expression following the differentiation protocol (Figure 4A). Like MNs derived from ALS patients, these isogenic *TARDBP* mutant MNs also exhibited shorter neurites than did MNs derived from healthy controls under *HB9::RPF*-infected live cell neurite staining (Figure 4B). Moreover, *PHOX2B* mRNA expression was also downregulated (Figure 4C), suggesting that normal *PHOX2B* expression depends on conserved TDP-43 function. Axon length and *PHOX2B* mRNA expression did not change between control MNs and genome-editing non-targeting control MNs that only had silent mutations (Figure S2B). Axon branching of iPSC-derived *TARDBP* mutant MNs were increased compared with those of healthy control MNs in live cells, which were consistent with our previous report (Akiyama et al., 2019) (Figure S2C).

TDP-43 binds and stabilizes *PHOX2B* mRNA in neurites

RIP (RNA immunoprecipitation) with anti-TDP-43 antibodies revealed that TDP-43 was bound to *PHOX2B* mRNA (Figures 5A and 5B). The GFP-tagged WT and mutant TDP-43 (p.A315T, p.M337V, and p.G376D) immunoprecipitated using anti-GFP antibodies were found to bind *PHOX2B* mRNA (Figures S3A and S3B), suggesting that the ALS-associated mutations did not eliminate TDP-

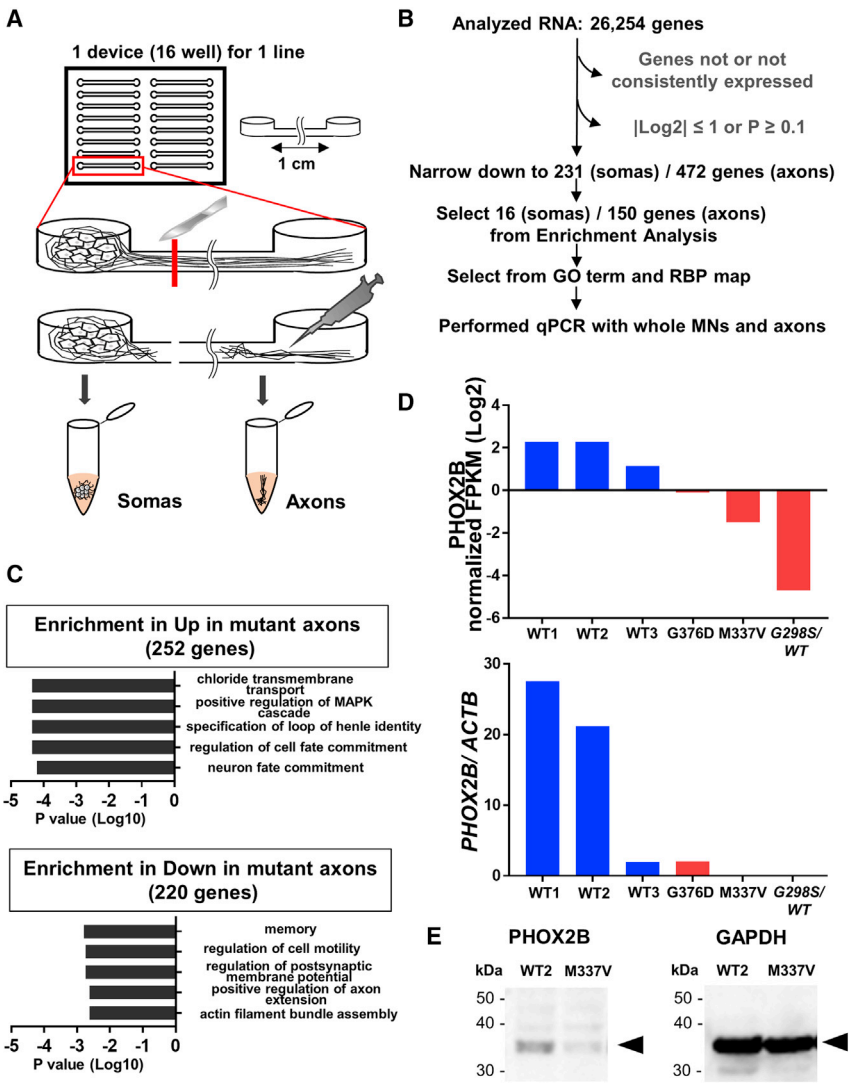

Figure 3. Expression of *PHOX2B* was reduced in *TARDBP* mutant MNs compared with control MNs

(A) Schema illustrating isolation of somas and axons from iPSC-derived MNs using microfluidic chambers.

(B) Selection of candidate genes associated with *TARDBP* mutation-induced axonal pathology based on RNA-seq. The number of candidates was reduced from 26,254 to 231 in somas and 472 in axons on normalized fragments per kilobase of the exon model per million mapped fragments (FPKM) values | log2| > 1 and p < 0.1 (Student's t test). From enrichment analysis, 16 genes (all genes were downregulated in the mutant) were significantly changed in the soma fraction, and 150 genes (103 genes were upregulated and 47 genes were downregulated in the mutant) were in the axon fraction. *PHOX2B* was selected from GO term (related to nerves, axons, transport, cytoskeleton, and inflammation), RBP map, and qPCR. See also Tables S4, S5, S6, and S7.

(C) Enrichment analysis revealed significant upregulation of transcripts associated with chloride transmembrane transport, the MAPK cascade, and cell or neuron fate commitment in *TARDBP* mutant axons (252 genes, upper panel). By contrast, transcripts associated with memory, cell motility, postsynaptic membrane potential, and axon- or actin-related genes were significantly downregulated (220 genes, lower).

(D) *PHOX2B* was selected from RNA-seq results. The upper graph shows RNA-seq results (normalized FPKM) and the lower graph shows qPCR results (*PHOX2B/ACTB* [β-actin]). *PHOX2B* normalized FPKM were decreased in *TARDBP* mutant axons. *PHOX2B* mRNA expression was also equal or decreased in the mutant axons with qPCR using RNA samples for RNA-seq under independent triplicates per sample. See also Figure S1B for qPCR results of N345K.

(E) PHOX2B protein expression was examined by western blotting. Expression of PHOX2B (32 kDa, arrowhead) was substantially lower in *TARDBP* mutant MNs (M337V) compared with that in healthy control MNs (WT2), consistent with the mRNA expression pattern measured by RNA-seq and qPCR. GAPDH (37 kDa, arrowhead) was used as the gel loading control.

43's binding ability to the *PHOX2B* mRNA. Therefore, *PHOX2B* mRNA downregulation is not likely to result from the lack of recognition by mutant TDP-43. Moreover, *TARDBP* mRNA KD using small interfering RNA (siRNA) (si-*TARDBP*, siT) also decreased the level of *PHOX2B* mRNA in SH-SY5Y cells (Figure 5C).

To further investigate the relationship between *PHOX2B* mRNA downregulation and *TARDBP* mutations, we compared the subcellular localization of *PHOX2B* mRNA between WT and mutant MNs by single-molecule RNA fluorescence *in situ* hybridization (smFISH). Although some *PHOX2B* mRNA red fluorescence was localized in the axons of healthy control MNs (WT1), this signal was absent from the axons of mutant MNs (Q343R, M337V, and G376D) (Figure 5D, inset). To determine whether this change in subcellular expression is due to *PHOX2B* mRNA instability, mRNA stability assays were conducted using actinomycin D. Concentration and treatment time of actinomycin D were the same between control and *TARDBP* mutant MNs, and there was no clear damage to the cells. After 1 h of actinomycin D treatment, expression of endogenous *PHOX2B* mRNA in *TARDBP* mutant MNs was significantly reduced, whereas it was maintained in control MNs (Figure 5E).

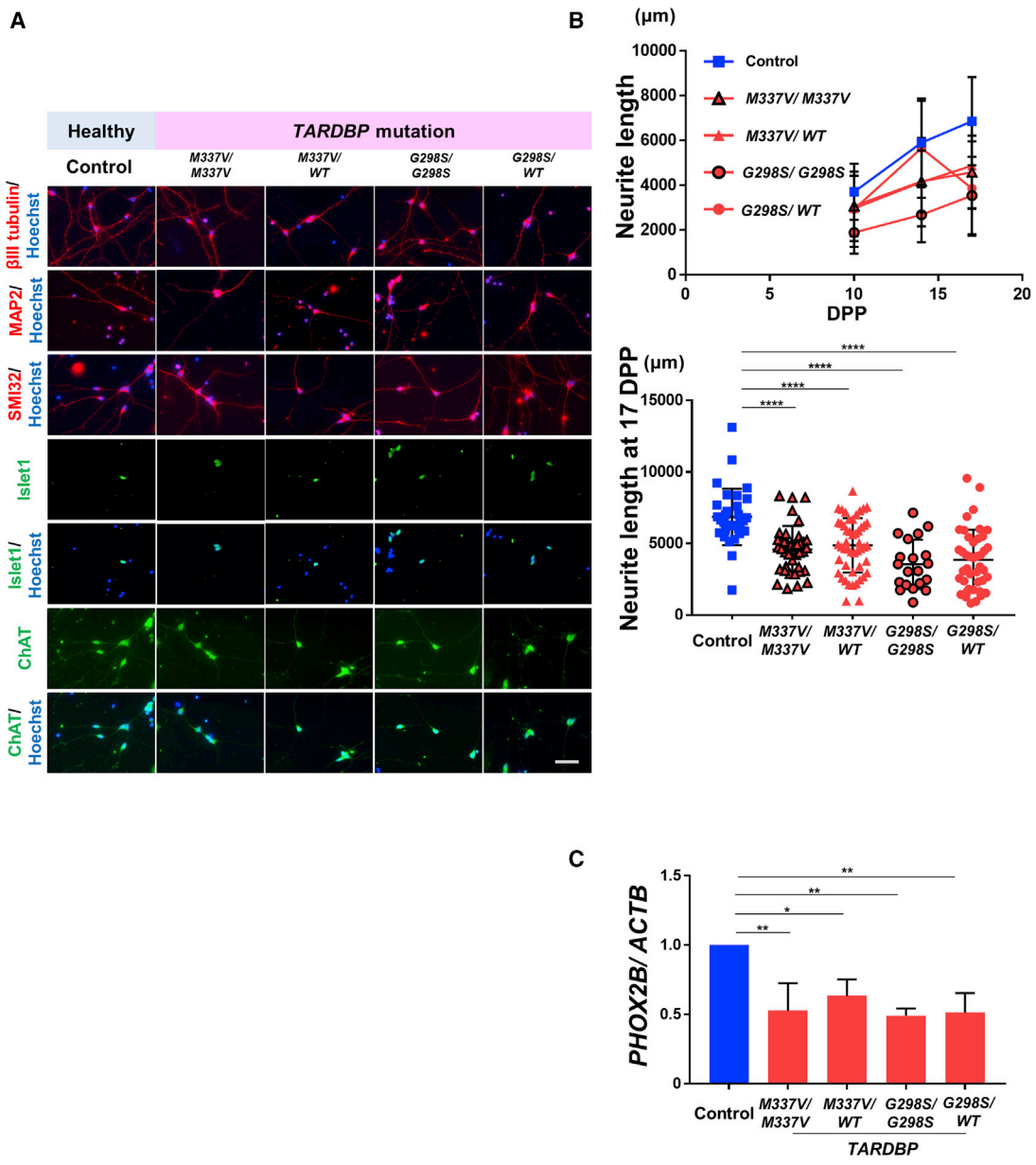

Figure 4. Validation of *PHOX2B* mRNA downregulation by *TARDBP* mutations in isogenic MNs

(A) MNs differentiated from *TARDBP* mutant isogenic iPSCs also expressed neuronal and MN-specific markers. Scale bar, 50 μm.

(B) MNs derived from *TARDBP* mutant isogenic iPSCs also exhibited significantly shorter neurites than did MNs derived from control (WT) iPSCs. Neurites were stained with RFP by infection with *HB9::RFP* lentivirus vector. From 20 to 77 neurites were analyzed per group depending on time post differentiation for one experiment. Two-way ANOVA with post hoc Tukey HSD tests. ****P < 0.0001.

(C) *PHOX2B* mRNA expression was also significantly lower in MNs derived from *TARDBP* mutant isogenic iPSCs compared with those in control MNs at 7 dpp. n = 3 independent triplicates per group. One-way ANOVA with post hoc Tukey HSD tests. **p < 0.01, *p < 0.05. See also Figure S2 and Tables S1–S3.

On the contrary, *GAPDH* mRNA as the negative control gene did not decrease during 6 h of actinomycin D treatment in both control and *TARDBP* mutant MNs (Figure S3C). These results indicate that *TARDBP* mutations reduce *PHOX2B* mRNA stability.

PHOX2B regulates iPSC-derived MN neurite length

To investigate whether *PHOX2B* can regulate neurite length, iPSC-derived MNs were transfected with siRNA for *PHOX2B* KD (si*PHOX2B*, siP) and their neurites were compared with those of a negative control siRNA

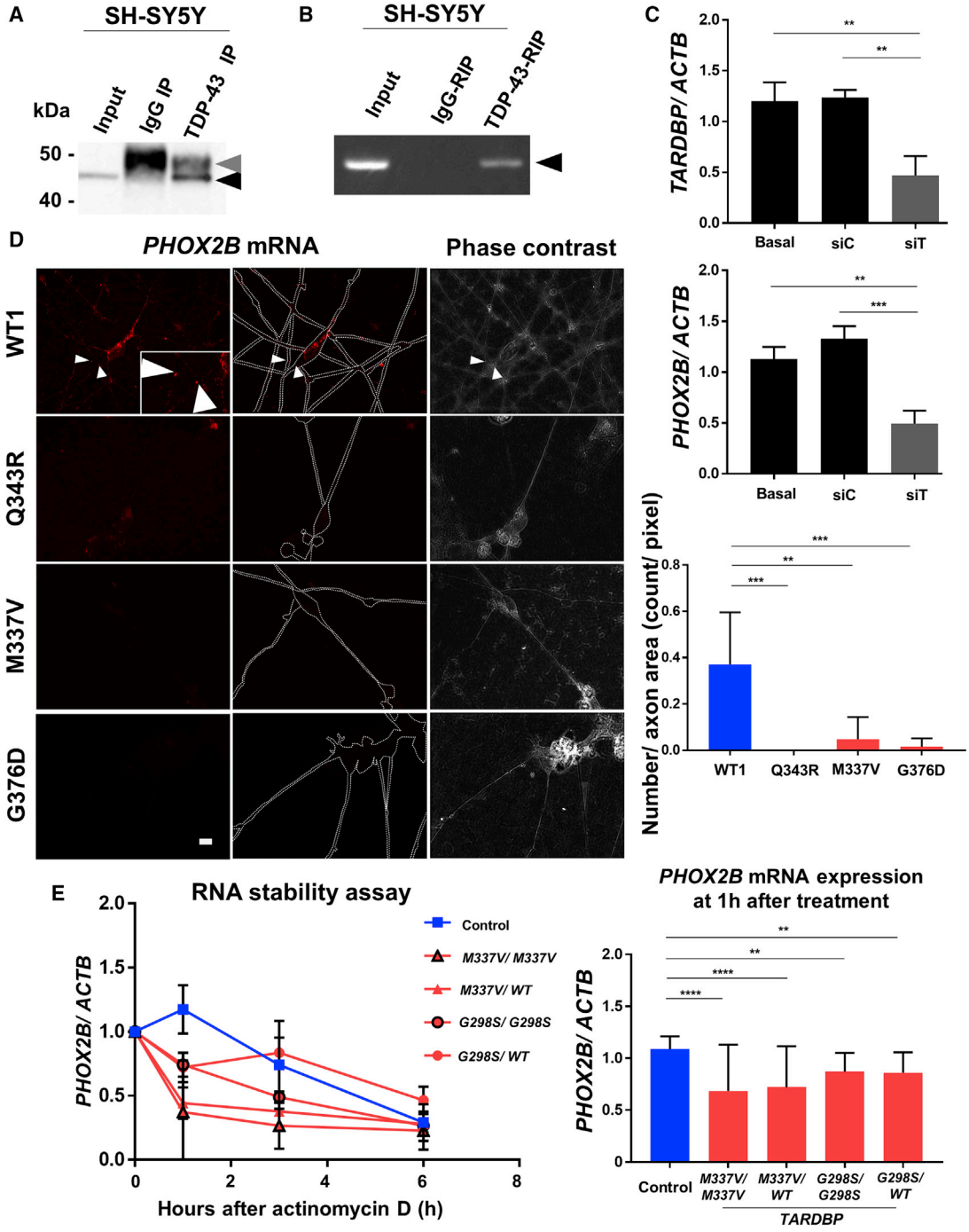

Figure 5. TDP-43 bound and stabilized *PHOX2B* mRNA in neurites

(A) Endogenous TDP-43 (43 kDa, black arrowhead) was detected by western blotting in SH-SY5Y cell immunoprecipitation samples using anti-TDP-43 antibody. The upper band indicates the immunoglobulin G (IgG) heavy chain (50 kDa, gray arrowhead). The lower IgG light chain band (25 kDa) was not shown.

(B) *PHOX2B* mRNAs (black arrowhead) were amplified by PCR from SH-SY5Y cell RIP samples using anti-TDP-43 antibody. *PHOX2B* mRNA bound to TDP-43.

(C) Transduction of siRNA (si*TARDBP*, siT) knocked down *TARDBP* mRNA in SH-SY5Y cells (upper graph), wherein *PHOX2B* mRNA also decreased (lower graph). n = 3 independent triplicates. One-way ANOVA with post hoc Tukey HSD tests. ***p < 0.001, **p < 0.01.

(legend continued on next page)

(siControl, siC) transfected MNs. Transfection of siP to healthy control MNs (WT1) substantially reduced *PHOX2B* expression at both mRNA and protein levels compared with WT1 MNs with siControl (Figures 6A and 6B). Furthermore, siP but not siC transfection substantially reduced neurite length compared with healthy control MNs (WT1 and WT2) at 21 dpp (Figures 6C and 6D).

phox2b affects zebrafish spinal axon length, morphology, and motor functions

To examine if *PHOX2B* can also influence MN neurite length *in vivo* and influence motor function, we compared MN morphology and escape behavior between control and *phox2b* KD zebrafish. Because zebrafish embryos are transparent, spinal MNs are easy to observe by fluorescent protein labeling with motor neuron-specific *HB9* promoter (Stil and Drapeau, 2016), and zebrafish *phox2b* is highly homologous to the human *PHOX2B* (Pei et al., 2013). *phox2b* KD was induced by injection of a splice-blocking morpholino into zebrafish fertilized eggs (Figure S4A). The splice-blocking morpholino oligonucleotide (MO) targets splice junction of *phox2b* second exon and blocks splicing of the intron 2, including a stop codon, resulting in an incomplete *phox2b* translation and *phox2b* KD (Pei et al., 2013). Consistent with cell culture studies, zebrafish injected with the splice-blocking MO exhibited significantly shorter spinal axons (and more axonal spines) than controls injected with mismatch control MO at both 2 and 3 days post fertilization (dpf) (Figures 7A–7C). Moreover, axonal spines were thicker and abnormal ectopic axons were increased in KD zebrafish at 3 dpf (Figures 7A and 7D). Finally, motor functions of MO-injected zebrafish were analyzed by comparing touch-evoked escape responses at 2 dpf. Consistent with disruption of MN morphology, zebrafish injected with the splice-blocking MO were unresponsive to tail stimulation (Figures 7E, 7F, and S4B). Moreover, *Phox2b* expression in *hSOD1*^{G93A} transgenic (Tg) rats was reduced in the lumbar spinal cord anterior horn cells compared with the non-Tg rats (Figure 7G). The *in vivo* expression of *Phox2b* was decreased in the MNs of the ALS model.

DISCUSSION

In this study, RNA-seq analysis revealed diminished transcription of *PHOX2B* in iPSC-derived MNs that include the ALS-associated *TARDBP* mutation; this finding was associated with neurite length shortening and reduced motor function both *in vivo* and *in vitro*. Both neurite length shortening and reduced motor functions were reported previously in experimental models of ALS (Akiyama et al., 2019; Babin et al., 2014; Egawa et al., 2012; Fujimori et al., 2018) and these findings were reproduced in this study. Reduced neurite length in MNs derived from the iPSCs of ALS patients harboring *TARDBP* mutations, such as p.M337V or p.Q343R, has been observed previously (Fujimori et al., 2018). To confirm and extend these findings, neurite length was significantly shorter in MNs derived from both patient-derived and isogenic mutant iPSCs than that from healthy control iPSCs, indicating that reduced neurite length is a common feature of MNs with ALS-associated *TARDBP* mutations. Similarly, phenotypes associated with the *phox2b* KD zebrafish were similar to those identified in our previous reports describing the impact of *Fos-B* overexpression (Akiyama et al., 2019). Shorter axon length and increased axon branching have been reported as pathological hallmarks of ALS-associated gene mutations in zebrafish (Babin et al., 2014).

PHOX2B is the causative gene for congenital central hypoventilation syndrome (Cain et al., 2017) but has not been directly linked to ALS. PHOX2B protein is a highly conserved transcription factor expressed mainly in neural cells and is essential for neural crest formation (Pattyn et al., 1999). Phox2b, a transcription factor that is expressed in intracranial and upper cervical MNs of embryonic mice, was also reported to induce neural differentiation from neural progenitor cells (Mazzoni et al., 2013; Nagashimada et al., 2012; Song et al., 2006). In adults, *Phox2b* mRNA is expressed in mouse spinal anterior horn cells according to the Allen Brain Atlas (http://portal.brain-map.org/). In this study, it was revealed that *Phox2b* is expressed in normal rat lumbar spinal cord anterior horn cells (Figure 7G). These characteristics suggest potential functions

(D) Results of smFISH demonstrating *PHOX2B* mRNAs in the axons of control MNs but not *TARDBP* mutant MNs. The two left columns show *PHOX2B* mRNA fluorescence (red). The edges of the MNs are indicated by white dotted lines. Right columns show bright-field images of the same MNs. *PHOX2B* mRNA was detected in healthy control MN (WT1) axons (white arrowheads and inset) but was barely detectable in mutant (Q343R, M337V, and G376D) MN axons. Scale bar, 10 μm. Quantitative evaluation (right graph) was performed by dividing the red particles of *PHOX2B* mRNA in the axons by the number of pixels in the axon area of the phase-contrast image. The number of the particles or axon areas revealed that *PHOX2B* mRNA was detected in WT1 MN axons significantly more than in *TARDBP* mutant MN axons. n = 3–9 fields. One-way ANOVA with post hoc Tukey HSD tests. ***p < 0.001, **p < 0.01.

(E) RNA stability assay conducted in MNs at 7 dpp. *PHOX2B* mRNA expression rapidly decreased at 1 h of actinomycin D treatment in *TARDBP*$^{M337V/M337V}$, *TARDBP*$^{M337V/WT}$, *TARDBP*$^{G298S/G298S}$, and *TARDBP*$^{G298S/WT}$ MNs, whereas this same level of degradation required 3 h of actinomycin D treatment in control MNs. Statistical analysis performed with n = 3, at 0 and 1 h, independent triplicates per treatment group. Two-way ANOVA with post hoc Tukey HSD tests. ****p < 0.0001, **p < 0.01. See also Figure S3 and Tables S2 and S3.

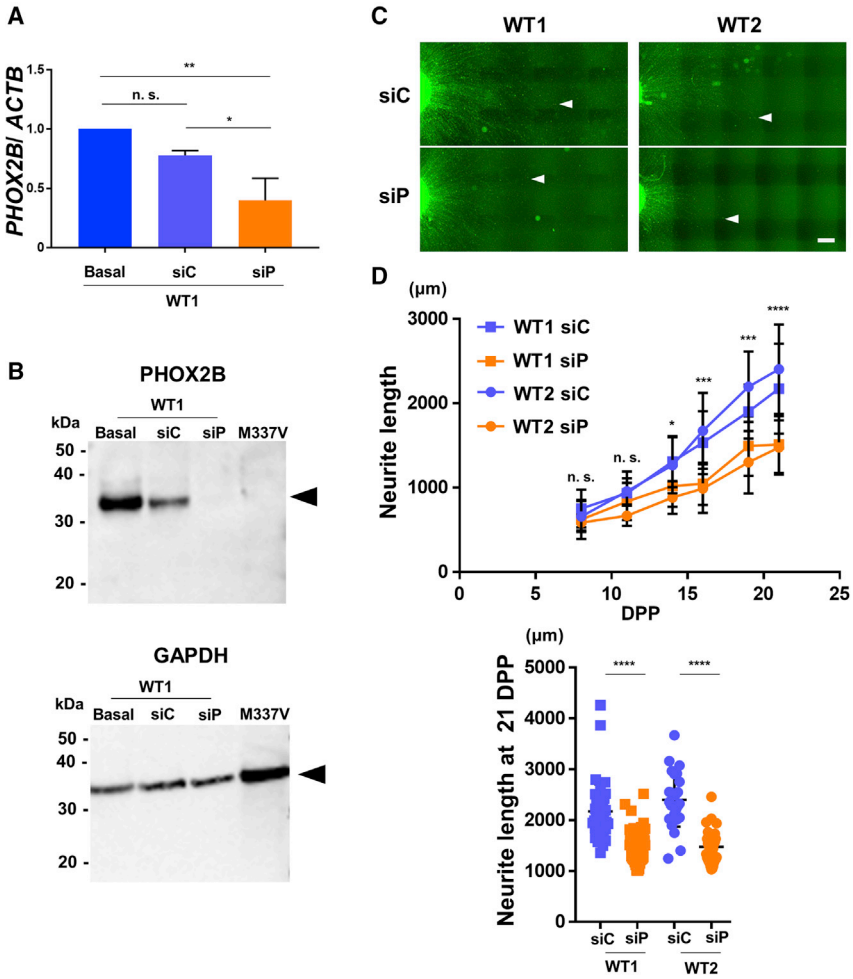

Figure 6. *PHOX2B* knockdown in control MNs reduced neurite length

(A) Control MNs were transfected with siP or siC at 3 dpp and RNA extracted at 7 dpp for expression analysis by qPCR. MNs transfected with siP showed an approximately 50% reduction in *PHOX2B* expression compared with MNs transfected with siC. Statistical analysis performed on n = 3 independent triplicates. One-way ANOVA with post hoc Tukey HSD tests. $^{**}p < 0.01$, $^{*}p < 0.05$.

(B) Knockdown efficiency of PHOX2B by siRNA was examined by western blotting. The reduction in PHOX2B (32 kDa, arrowhead) was comparable with that observed in M337V *TARDBP* mutant MNs. GAPDH (37 kDa, arrowhead) was used as the gel loading control.

(C) Knockdown of PHOX2B in healthy control MNs (WT1 and WT2) reduced neurite length compared with MNs transfected with siC at 21 dpp. The white arrowheads indicate the most distal neurite ends. Scale bar, 300 μm.

(D) The upper graph shows neurite length changes over time. Twenty-five to 80 neurites were analyzed per group for one experiment, depending on the time post differentiation. A comparison between the siC and siP groups showed that the neurite length significantly decreased in the siP group from day 14. The lower graph shows quantitative analysis at 21 dpp. MNs transfected with siP significantly reduced neurite length compared with MNs transfected with siC at 21 dpp. Repeated measures ANOVA with post hoc Tukey HSD tests for comparison between siC and siP. Two-way ANOVA with post hoc Tukey HSD tests for among each cell lines. $^{*}p < 0.05$, $^{**}p < 0.01$, $^{***}p < 0.001$, $^{****}p < 0.0001$. See also Tables S2 and S3.

of PHOX2B in MNs, a notion supported by reduction of MN axonal length and motor dysfunction by *PHOX2B* KD in this study. As per our knowledge, PHOX2B has not been mentioned in the published dataset using ALS autopsy samples in the Gene Expression Omnibus. This might be because the autopsy samples reflect the disease's end stage, whereas PHOX2B suppression and axonal pathology reflect the disease's early stage. Moreover, it has been reported that oculomotor and trochlear MNs highly express PHOX2A (Allodi et al., 2019), which is structurally similar to PHOX2B, and reported to form heterodimers with PHOX2B *in vitro* (Di Lascio et al., 2016). Oculomotor and trochlear motor neurons show a better survival rate than spinal cord MNs in ALS (An et al., 2019), thus high PHOX2A expression in these cells might serve to protect them from cell death associated with ALS. In this study, expression of *PHOX2A* was also downregulated in *TARDBP* mutant axons (RNA-seq; fold change = 0.1085, p = 0.0104, Table S5); interestingly, the expression of PHOX2A protein in mutant MNs was indistinguishable from that detected in the WT (data not shown). PHOX2B is highly expressed in noradrenergic neurons or oculomotor neurons that are maintained for a long time during ALS progression (Allodi et al., 2019; Fan et al., 2018). These results suggest that PHOX2B may normally serve to reduce MN vulnerability and to increase resilience of noradrenergic neurons and/or oculomotor neurons in patients with ALS.

TDP-43 mutations are known to be involved in the pathogenesis of ALS through a variety of mechanisms (Ling et al., 2013). In this study, TDP-43 mutations seem to be involved in the decreased stability of *PHOX2B* mRNA, consistent with the presence of a TDP-43 binding consensus sequence in its 3′ UTR. However, the mechanisms underlying the stability of *PHOX2B* mRNA remain uncertain. While we observed no changes with respect to TDP-43 and *PHOX2B* mRNA binding interactions, there may be differential expression of specific mRNA isoforms in the WT compared with the mutant MNs. There are at

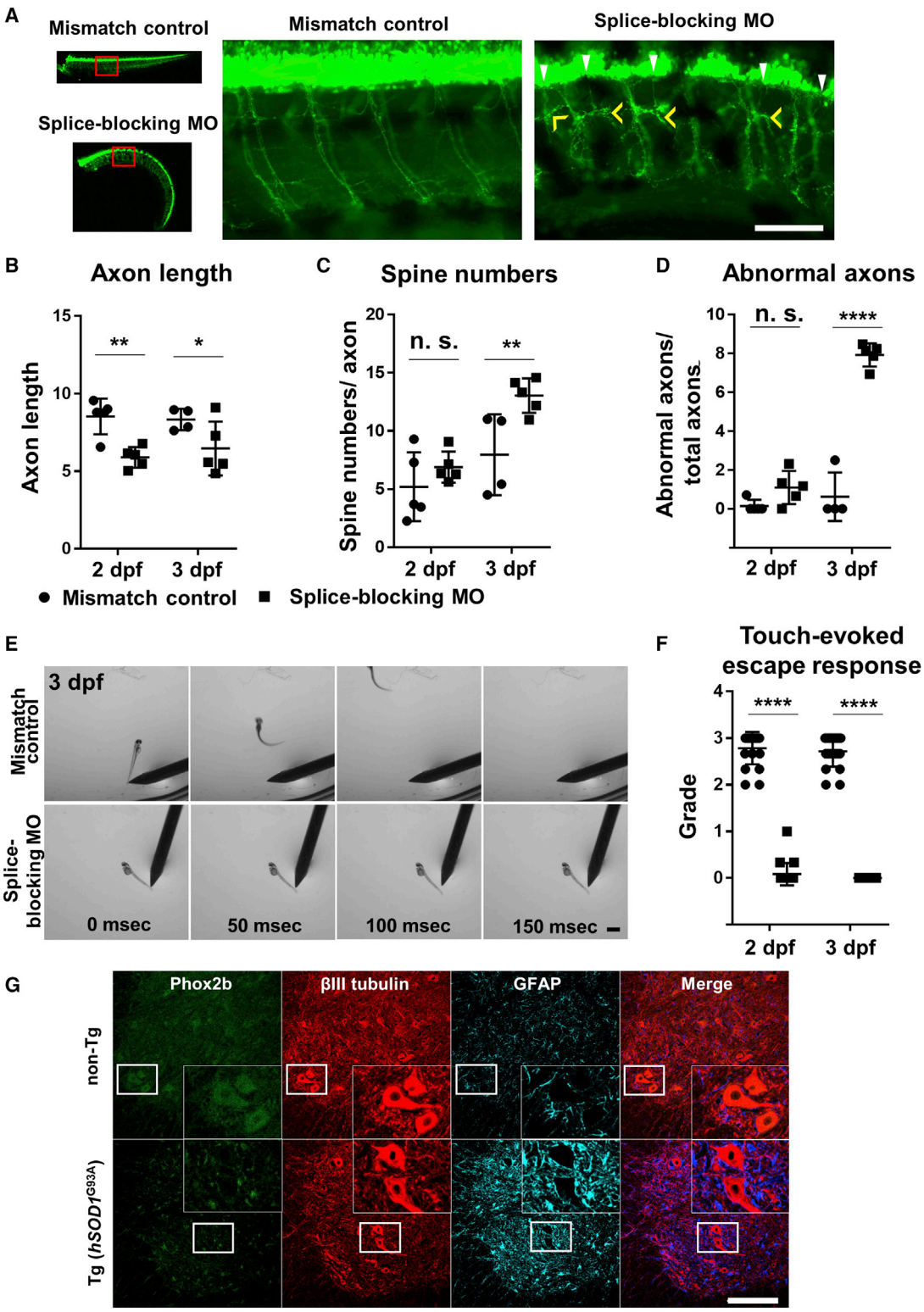

Figure 7. *phox2b* knockdown in zebrafish reduces spinal axon length and impairs motor function

(A) Zebrafish embryos injected with a splice-blocking MO for *phox2b* (lower column) have shorter spinal axons and increased axonal spines compared with those injected with mismatch control MO (upper column) at 3 dpf. In zebrafish injected with the splice-blocking MO, axonal spines also became thicker (yellow arrow heads), and abnormal ectopic axons (white arrow heads) were detected. Scale bar, 100 μm.

(legend continued on next page)

least two isoforms of *PHOX2B* that can be distinguished by the lengths of their respective 3′ UTRs (Cardani et al., 2018); the biphasic degradation of *PHOX2B* mRNA observed here (Figure 5E) may be directly related to factors distinguishing these mRNAs. Likewise, isoforms encoding characteristic sequences of the mutant MNs may be more easily degraded than those identified in the WT.

This study has several limitations. First, the selection of candidate genes associated with *TARDBP* mutation-induced axonal pathology did not consider some genes associated with other pathological hypotheses. Second, both iPSC-derived MNs and zebrafish were observed at the early stages of development, while ALS is an adult-onset disease. Third, *phox2b* KD in zebrafish was not specific to MNs. In addition, PHOX2B was reported to be expressed mainly in the neural crest during differentiation (Fan et al., 2018), so motor deficits in zebrafish embryos may be due to restricted development of other neural pathways. Moreover, although we attempted to overexpress *PHOX2B* by transfection with lentiviral vectors expressing PHOX2B with a C-terminal GFP tag under the cytomegalovirus promoter, the total amount of *PHOX2B* mRNA remained unchanged, possibly because the total mRNA level of *PHOX2B* in the MNs is strictly controlled or due to the effects of lentiviral transfection (data not shown). In neuroblastoma, *PHOX2B* mRNA has been reported to transactivate itself by binding to its own promoter region (Cargnin et al., 2005). However, this transactivation disappears in the presence of *PHOX2B* mutations due to their dominant-negative effect (Di Lascio et al., 2018). The sequence of lentiviral vectors expressing GFP-tagged PHOX2B was confirmed as expected (data not shown), thus ruling out the possibility of a dominant-negative effect. The mutant TDP-43 knockin mouse model with early MN-selective degeneration (Ebstein et al., 2019) should be used in future studies for analyzing expression and localization changes of PHOX2B.

In conclusion, PHOX2B downregulation found in RNA-seq using iPSCs derived MNs mediates *TARDBP* mutation-induced loss of axonal resilience, suggesting PHOX2B pathways as potential therapeutic targets for ALS. We speculate that the decreased *PHOX2B* mRNA and protein expression in *TARDBP* mutant MNs reduces this local translation and retrograde transport in response to various stimuli, which in turn leads to deficient expression of the still unknown PHOX2B target genes required for neurite length elongation, axonal maintenance, and/or MN survival. Further studies should explore downstream factors of PHOX2B that are related to MN vulnerability of ALS.

EXPERIMENTAL PROCEDURES

Creation of iPSC lines

The creation of human iPSC lines was approved by the Tohoku University ethics review board (Nos. 2014-1-733 and 2016-1-814) and Keio University ethics review board (No. 20080016). See also supplemental experimental procedures

Collection and maintenance of iPSCs

All iPSC lines used in this study (Table S1) were cocultured with SNL 76/7 murine fibroblast feeder cells (ECACC) pretreated with 10 μg/mL of mitomycin C (Sigma) and maintained at 37°C and 3% CO_2.

Differentiation into MNs

iPSCs were differentiated into MNs according to a previous report (Fujimori et al., 2017) (see also supplemental experimental procedures). The second MPCs were cultured in 96-well v-bottom plates (Sumitomo Bakelite) at 1×10^4 cells/well to generate neurospheres

(B) Quantitative analysis of Venus-positive spinal axon length. Spinal axon length was normalized to total spinal cord length. Zebrafish embryos injected with the splice-blocking MO exhibited significantly shorter spinal axons at 2 dpf than zebrafish embryos injected with mismatch control MO. n = 4–5 animals per group. Two-way ANOVA with post hoc Tukey HSD tests. **p < 0.01, *p < 0.05.

(C) Quantitative analysis of Venus-positive axonal spine numbers. Zebrafish embryos injected with the splice-blocking MO exhibited significantly more spines per axon at 3 dpf than zebrafish embryos injected with mismatch control MO. The average spine numbers of 13–15 axons per animal was compared in 4–5 animals per group. Two-way ANOVA with post hoc Tukey HSD tests. **p < 0.01.

(D) Quantitative analysis of Venus-positive abnormal axons. Axons connecting to ectopic axons or with spines as thick as or thicker than the caudal MNs were defined as abnormal. Zebrafish embryos injected with the splice-blocking MO had significantly more abnormal axons at 3 dpf than zebrafish embryos injected with mismatch control MO. n = 4–5 animals per group. Two-way ANOVA with post hoc Tukey HSD tests. ****p < 0.0001.

(E) The effects of *phox2b* KD on motor functions were assessed by comparing touch-evoked escape responses at 3 dpf. Zebrafish embryos injected with the splice-blocking MO (lower column) were unresponsive to tail stimulation. Scale bar, 1000 μm.

(F) Quantitative analysis of touch-evoked escape response grade. At 2 dpf, no zebrafish embryos injected with the splice-blocking MO swam away after tail stimulation, whereas a few reacted by tail flicking. At 3 dpf, all were unresponsive to stimulation. n = 20 per treatment group under triplicates for each animal. Two-way ANOVA with post hoc Tukey HSD tests. ****p < 0.0001. See also Figure S4.

(G) In *hSOD1*^{G93A} Tg rats, Phox2b (green) expression was reduced in βIII tubulin (red) positive lumbar spinal cord anterior horn cells compared with the non-Tg rats. GFAP (glial fibrillary acidic protein, cyan) positive astrocytes show very faint Phox2b staining in non-Tg rats. The figure's lower end represents the ventral side. Scale bar, 200 μm.

for performing neurite length measurements and RNA-seq analysis. The second MPC neurospheres were then cultured on 24-well thin-bottom plates (Iwaki) coated as above to measure neurite length or in microfluidic devices (Jiksak Bioengineering) (Kawada et al., 2017) for axon/soma isolation and analysis by RNA-seq. The microfluidic devices were obtained from Prof. Teruo Fujii and Dr. Jiro Kawada.

Neurite length analysis of iPSC-derived MNs

iPSC lines were differentiated into MNs as described above and infected with lentivirus vector (*HB9::Venus*, *EF-1α::Venus*, or *HB9::RFP*). Neurite length was measured every 2–4 days from the neurite end to the sphere edge using the BZ-X700 measurement tool (Keyence). Transfection of siRNA si*PHOX2B* (Ambion) were performed every 3 days starting on day 22 of differentiation using RNAiMax (Thermo Fisher). Silencer Select siRNA (Ambion) was used as the control (siC).

RNA-seq sample collection from microfluidic devices

Prepared samples for RNA-seq were iPSC-derived MNs of healthy controls (WT1, WT2, and WT3, which was a WT2 technical duplicate), familial ALS with *TARDBP* mutations (M337V and G376D), and *TARDBP* isogenic MNs constructed from WT1 (*TARDBP*$^{M337V/M337V}$, *TARDBP*$^{M337V/WT}$, *TARDBP*$^{G298S/G298S}$, and *TARDBP*$^{G298S/WT}$). In brief, iPSCs were differentiated into MPC spheres as described above and plated in one well of a microfluidic device containing two wells at opposite ends. With this plating strategy, only axons extended to reach to the opposite well, usually within 21 days. Neurites 450 μm or more distant from the cell body, defined as axons according to a previous report (Taylor et al., 2005), were separated from soma using medical scalpels, and both axon and soma fractions were collected. In total, 8–16 wells were obtained from each cell line.

RNA extraction

RNA was extracted for RNA-seq and qPCR using the QIAGEN RNA Micro Kit according to the manufacturer's protocol.

RNA-seq and analysis

The TruSeq Stranded mRNA LT Sample Prep Kit (Illumina) was used for preparation of the soma RNA-seq library and the SMARTER Seq v4 Ultra Low Input RNA Kit for the axonal RNA-seq library (Takara). RNA-seq was performed using the HiSeq 2500 system (Illumina) in rapid mode with 51 bp single-end sequencing. UCSC hg19 and RefSeq were used for the reference human genome and gene model. For gene expression analysis, sequence FASTQ files were mapped to the reference human genome using TopHat (v.2.1.1). FPKM (fragments per kilobase of the exon model per million mapped fragments) was calculated as the gene expression levels from the mapping file using Cufflinks (v.2.2.1).

Selection of disease-related candidate genes from RNA-seq

Two batches of RNA-seq (the non-isogenic MNs and isogenic MNs) were integrated and analyzed. Samples containing some genes suspected of degrading RNA (e.g., the expression pattern of only the 3′ UTR was displayed) in the evaluation using IGV (Integrative Genomics Viewer: https://software.broadinstitute.org/software/igv/home) were excluded from the analysis. The results were analyzed using Subio for each of the axons and somas (see also supplemental experimental procedures). Normalized FPKM values were compared between controls and *TARDBP* mutations in axon or soma fractions, and differentially expressed genes were picked up with $|\log2| > 1$ (fold changes < 0.5, 2 < fold changes) and $p < 0.1$ (Student's t test). Enrichment analysis was also performed using Subio software (v.1.24), and enriched GO term categories were selected by number in Category < 100, number Overlaps > 3, and $p < 0.05$. TDP-43 binding sequences were searched using RBP map (http://rbpmap.technion.ac.il) (Figure 3B).

qPCR

Extracted RNA was reverse transcribed to cDNA using the QuantiTect Reverse Transcription Kit (QIAGEN). Quantitative real-time PCR was performed using the SsoFast EvaGreen Supermix (Bio-Rad) and analyzed using a CFX96 Real-Time PCR Detection System (Bio-Rad). Primer sets used for each target gene are listed in Table S2. ACTB was used as the internal control gene. All qPCRs were performed in triplicate for each sample. Candidate genes were quantified using a standard curve. Expression levels are shown as mean and standard error.

Western blotting

Western blotting was performed as described in our previous report (Akiyama et al., 2019). See also supplemental experimental procedures.

RNA stability assay

To determine the impact of endogenous mutations on the stability of *PHOX2B* mRNA, iPSC-derived MNs derived from *TARDBP* isogenic lines were treated with 10 μg/mL actinomycin D for 0, 1, 3, and 6 h; three samples were collected for each line and in response to 0 and 1 h treatment conditions. RNA extraction and qPCR protocols were as described above.

Construction of lentivirus vectors

We used lentivirus vectors for fluorescent marking of MNs. Lentivirus vectors *HB9::Venus*, *FE-1α::Venus*, and *HB9::RFP* were constructed as described in our previous report (Akiyama et al., 2019). The self-inactivating (SIN) vector plasmid and the packaging vector plasmid were provided by Dr. Hiroyuki Miyoshi (Shimojo et al., 2015). Venus is a modified GFP developed by Dr. Atsushi Miyawaki of RIKEN (Nagai et al., 2002). RFP was permitted for use by UCSD (University of California San Diego).

Axon length and spine-counting analyses in *phox2b* KD zebrafish

Zebrafish were maintained at Tokai University under approved protocols (approval No. 195001). Endogenous *phox2b* KD zebrafish were created by injection of a splice-blocking MO that was designed to induce aberrant splicing of zebrafish *phox2b* as described previously (Pei et al., 2013). The transgenic zebrafish line hb9:Venus (Nakano et al., 2010) was used to visualize MNs *in vivo*. The

fertilized eggs of the hb9:Venus × RIKEN WT zebrafish strain were injected with 4 pg of the splice-blocking MO or mismatched MO as a control. Venus-positive axon length was measured from the beginning of the spinal cord to the end. Ectopic axons, axons connecting to ectopic axons, and axons with thicker spines than caudal MNs were defined as abnormal. Data are expressed as mean and standard error and were compared by two-way ANOVA with post hoc Tukey HSD tests.

Motor function analyses of *phox2b* KD zebrafish

The effects of *phox2b* KD on motor function were assessed by comparing touch-evoked escape responses in WT zebrafish injected with mismatch control MO at 2–3 dpf. Touch-evoked escape responses were graded (0, no movement; 1, flicker of movement but no swimming; 2, movement away from probe but with impaired swimming; 3, normal swimming) as described previously (Telfer et al., 2010) and performed in triplicate for each subject (n = 20 per treatment group). Data are expressed as mean and standard error and were compared by two-way ANOVA with post hoc Tukey HSD tests.

Statistical analysis

GraphPad Prism 7.04 (MDF) was used for all statistical analyses. Data are expressed as mean and standard error and were compared among treatment groups by one-way, two-way, or repeated measures ANOVA as indicated with post hoc Tukey HSD tests for pairwise comparisons. A p value of < 0.05 (two-tailed) was considered statistically significant for all tests. Data with no significant differences are described as "n.s." The level of significance is indicated by the number of asterisks (*$p < 0.05$, **$p < 0.01$, ***$p < 0.001$, ****$p < 0.0001$).

Data and code availability

The accession number for the RNA-seq data reported in this paper is DDBJ (DNA DataBank of Japan): DRA011838.

SUPPLEMENTAL INFORMATION

Supplemental information can be found online at https://doi.org/10.1016/j.stemcr.2021.04.021.

AUTHOR CONTRIBUTIONS

S. Mitsuzawa, N.S., and M.A. wrote and revised the manuscript. All authors read the final manuscript. S. Mitsuzawa, N.S., T.A., and M.A. designed the experiments and interpreted the results. S. Mitsuzawa performed all experiments, except for iPSC establishment and rat experiments. A.T. established hiPSCs from ALS patients with *TARDBP* p.G376D mutation and S. Morimoto established and provided hiPSCs from ALS patients with *TARDBP* p.N345K mutation (Leventoux et al., 2020). M.I., T.S., and H. Okano helped in iPSC establishment. J.K., S.K., Y.I., and T.F. developed the microfluidic devices. T.A., K.I., and A.O. helped in maintenance of iPSCs and differentiation to MNs. N.N., H. Ono, R.O., and S.O. discussed and advised about all experiments. T.A., R.F., M.S., T.N., and K.N. helped in RNA-seq. N.S., T.A., A.N., and R.I. helped in genetic analysis of ALS patients. H.M. performed the zebrafish experiments. T.S. and H.W. performed the rat experiments.

DECLARATION OF INTERESTS

The authors declare no competing interests.

ACKNOWLEDGMENTS

The authors thank N. Sugeno, T. Hasegawa, Y. Takai, T. Misu, and M. Kato of the Department of Neurology, Tohoku University, for advice regarding this research; M. Suzuki, N. Shimakura, H. Shigihara, and A. Machii of the Department of Neurology, Tohoku University, for their technical assistance; K. Kuroda, M. Kikuchi, and M. Nakagawa of the Division of Cell Proliferation, Tohoku University, and A. Tabe of Subio for assistance with the RNA-seq procedure; S. Koyama, T. Kato, and Y. Suzuki for ongoing care of the G376D proband; H. Inoue, S. Yamanaka, and M. Nakagawa (Kyoto University) for donating hiPSC clones 409B2, 201B7, and CiRA00026; S. Nakamura and F. Ozawa for cells shipping and maintenance in Department of Physiology, Keio University; T. Niihori and Y. Aoki for genetic analysis; T. Kamei, T. Yamashita, and T. Matsuo of Takeda Pharmaceutical Company for their gift of *TARDBP* mutant isogenic iPSCs; A. Miyawaki and H. Miyoshi for donating lentivirus vectors; and University of California, San Diego ([UCSD], San Diego, USA) for permission to use their RFP; H. Momma for statistical advice; Y. Akiyama for the illustrations. We also thank the Biomedical Research Unit of Tohoku University Hospital for providing the locations to maintain hiPSCs. Zebrafish line Tg [hb9:Venus] and wild-type strain RIKEN WT were obtained from National BioResource Project, Zebrafish Core Institution, Japan. Sanger sequencing of zebrafish *phox2b* DNA constructs was performed by the Support Center for Medical Research and Education, Tokai University. This work was supported by JSPS KAKENHI grant No. JP20K16593. The authors would also like to thank Enago (www.enago.jp) for the English language review.

Received: July 17, 2020
Revised: April 26, 2021
Accepted: April 28, 2021
Published: May 27, 2021

REFERENCES

Akiyama, T., Suzuki, N., Ishikawa, M., Fujimori, K., Sone, T., Kawada, J., Funayama, R., Fujishima, F., Mitsuzawa, S., Ikeda, K., et al. (2019). Aberrant axon branching via Fos-B dysregulation in FUS-ALS motor neurons. EBioMedicine *45*, 362–378.

Allodi, I., Nijssen, J., Benitez, J.A., Schweingruber, C., Fuchs, A., Bonvicini, G., Cao, M., Kiehn, O., and Hedlund, E. (2019). Modeling motor neuron resilience in ALS using stem cells. Stem Cell Reports *12*, 1329–1341.

An, D., Fujiki, R., Iannitelli, D.E., Smerdon, J.W., Maity, S., Rose, M.F., Gelber, A., Wanaselja, E.K., Yagudayeva, I., Lee, J.Y., et al. (2019). Stem cell-derived cranial and spinal motor neurons reveal proteostatic differences between ALS resistant and sensitive motor neurons. Elife *8*, e44423.

Babin, P.J., Goizet, C., and Raldua, D. (2014). Zebrafish models of human motor neuron diseases: advantages and limitations. Prog. Neurobiol. *118*, 36–58.

Buratti, E., and Baralle, F.E. (2001). Characterization and functional implications of the RNA binding properties of nuclear factor TDP-43, a novel splicing regulator of CFTR exon 9. J. Biol. Chem. *276*, 36337–36343.

Cain, J.T., Kim, D.I., Quast, M., Shivega, W.G., Patrick, R.J., Moser, C., Reuter, S., Perez, M., Myers, A., Weimer, J.M., et al. (2017). Nonsense pathogenic variants in exon 1 of PHOX2B lead to translational reinitiation in congenital central hypoventilation syndrome. Am. J. Med. Genet. A *173*, 1200–1207.

Cardani, S., Di Lascio, S., Belperio, D., Di Biase, E., Ceccherini, I., Benfante, R., and Fornasari, D. (2018). Desogestrel down-regulates PHOX2B and its target genes in progesterone responsive neuroblastoma cells. Exp. Cell Res. *370*, 671–679.

Cargnin, F., Flora, A., Di Lascio, S., Battaglioli, E., Longhi, R., Clementi, F., and Fornasari, D. (2005). PHOX2B regulates its own expression by a transcriptional auto-regulatory mechanism. J. Biol. Chem. *280*, 37439–37448.

Coyne, A.N., Siddegowda, B.B., Estes, P.S., Johannesmeyer, J., Kovalik, T., Daniel, S.G., Pearson, A., Bowser, R., and Zarnescu, D.C. (2014). Futsch/MAP1B mRNA is a translational target of TDP-43 and is neuroprotective in a *Drosophila* model of amyotrophic lateral sclerosis. J. Neurosci. *34*, 15962–15974.

Di Lascio, S., Belperio, D., Benfante, R., and Fornasari, D. (2016). Alanine expansions associated with congenital central hypoventilation syndrome impair PHOX2B homeodomain-mediated dimerization and nuclear import. J. Biol. Chem. *291*, 13375–13393.

Di Lascio, S., Benfante, R., Di Zanni, E., Cardani, S., Adamo, A., Fornasari, D., Ceccherini, I., and Bachetti, T. (2018). Structural and functional differences in PHOX2B frameshift mutations underlie isolated or syndromic congenital central hypoventilation syndrome. Hum. Mutat. *39*, 219–236.

Ebstein, S.Y., Yagudayeva, I., and Shneider, N.A. (2019). Mutant TDP-43 causes early-stage dose-dependent motor neuron degeneration in a TARDBP knockin mouse model of ALS. Cell Rep. *26*, 364–373.e64.

Egawa, N., Kitaoka, S., Tsukita, K., Naitoh, M., Takahashi, K., Yamamoto, T., Adachi, F., Kondo, T., Okita, K., Asaka, I., et al. (2012). Drug screening for ALS using patient-specific induced pluripotent stem cells. Sci. Transl. Med. *4*, 145ra104.

Fan, Y., Chen, P., Raza, M.U., Szebeni, A., Szebeni, K., Ordway, G.A., Stockmeier, C.A., and Zhu, M.Y. (2018). Altered expression of Phox2 transcription factors in the locus coeruleus in major depressive disorder mimicked by chronic stress and corticosterone treatment in vivo and in vitro. Neuroscience *393*, 123–137.

Fujimori, K., Ishikawa, M., Otomo, A., Atsuta, N., Nakamura, R., Akiyama, T., Hadano, S., Aoki, M., Saya, H., Sobue, G., et al. (2018). Modeling sporadic ALS in iPSC-derived motor neurons identifies a potential therapeutic agent. Nat. Med. *24*, 1579–1589.

Fujimori, K., Matsumoto, T., Kisa, F., Hattori, N., Okano, H., and Akamatsu, W. (2017). Escape from pluripotency via inhibition of TGF-beta/BMP and activation of wnt signaling accelerates differentiation and aging in hPSC progeny cells. Stem Cell Rep. *9*, 1675–1691.

Huber, K., Karch, N., Ernsberger, U., Goridis, C., and Unsicker, K. (2005). The role of Phox2B in chromaffin cell development. Dev. Biol. *279*, 501–508.

Kapeli, K., Martinez, F.J., and Yeo, G.W. (2017). Genetic mutations in RNA-binding proteins and their roles in ALS. Hum. Genet. *136*, 1193–1214.

Kawada, J., Kaneda, S., Kirihara, T., Maroof, A., Levi, T., Eggan, K., Fujii, T., and Ikeuchi, Y. (2017). Generation of a motor nerve organoid with human stem cell-derived neurons. Stem Cell Rep. *9*, 1441–1449.

Leventoux, N., Morimoto, S., Hara, K., Nakamura, S., Ozawa, F., Mitsuzawa, S., Akiyama, T., Nishiyama, A., Suzuki, N., Warita, H., et al. (2020). Generation of an ALS human iPSC line KEIOi001-A from peripheral blood of a Charcot disease-affected patient carrying TARDBP p.N345K heterozygous SNP mutation. Stem Cell Res. *47*, 101896.

Ling, S.C., Polymenidou, M., and Cleveland, D.W. (2013). Converging mechanisms in ALS and FTD: disrupted RNA and protein homeostasis. Neuron *79*, 416–438.

Mackenzie, I.R., Bigio, E.H., Ince, P.G., Geser, F., Neumann, M., Cairns, N.J., Kwong, L.K., Forman, M.S., Ravits, J., Stewart, H., et al. (2007). Pathological TDP-43 distinguishes sporadic amyotrophic lateral sclerosis from amyotrophic lateral sclerosis with SOD1 mutations. Ann. Neurol. *61*, 427–434.

Mazzoni, E.O., Mahony, S., Closser, M., Morrison, C.A., Nedelec, S., Williams, D.J., An, D., Gifford, D.K., and Wichterle, H. (2013). Synergistic binding of transcription factors to cell-specific enhancers programs motor neuron identity. Nat. Neurosci. *16*, 1219–1227.

Mitsuzawa, S., Akiyama, T., Nishiyama, A., Suzuki, N., Kato, M., Warita, H., Izumi, R., Osana, S., Koyama, S., Kato, T., et al. (2018). TARDBP p.G376D mutation, found in rapid progressive familial ALS, induces mislocalization of TDP-43. eNeurologicalSci *11*, 20–22.

Nagai, T., Ibata, K., Park, E.S., Kubota, M., Mikoshiba, K., and Miyawaki, A. (2002). A variant of yellow fluorescent protein with fast and efficient maturation for cell-biological applications. Nat. Biotechnol. *20*, 87–90.

Nagashimada, M., Ohta, H., Li, C., Nakao, K., Uesaka, T., Brunet, J.F., Amiel, J., Trochet, D., Wakayama, T., and Enomoto, H. (2012). Autonomic neurocristopathy-associated mutations in PHOX2B dysregulate Sox10 expression. J. Clin. Invest. *122*, 3145–3158.

Nakano, Y., Fujita, M., Ogino, K., Saint-Amant, L., Kinoshita, T., Oda, Y., and Hirata, H. (2010). Biogenesis of GPI-anchored proteins is essential for surface expression of sodium channels in zebrafish Rohon-Beard neurons to respond to mechanosensory stimulation. Development *137*, 1689–1698.

Nishiyama, A., Niihori, T., Warita, H., Izumi, R., Akiyama, T., Kato, M., Suzuki, N., Aoki, Y., and Aoki, M. (2017). Comprehensive targeted next-generation sequencing in Japanese familial amyotrophic lateral sclerosis. Neurobiol. Aging *53*, 194 e191–194 e198.

Pattyn, A., Morin, X., Cremer, H., Goridis, C., and Brunet, J.F. (1999). The homeobox gene Phox2b is essential for the development of autonomic neural crest derivatives. Nature *399*, 366–370.

Pei, D., Luther, W., Wang, W., Paw, B.H., Stewart, R.A., and George, R.E. (2013). Distinct neuroblastoma-associated alterations of PHOX2B impair sympathetic neuronal differentiation in zebrafish models. PLoS Genet. *9*, e1003533.

Shimojo, D., Onodera, K., Doi-Torii, Y., Ishihara, Y., Hattori, C., Miwa, Y., Tanaka, S., Okada, R., Ohyama, M., Shoji, M., et al. (2015). Rapid, efficient, and simple motor neuron differentiation from human pluripotent stem cells. Mol. Brain *8*, 79.

Song, M.R., Shirasaki, R., Cai, C.L., Ruiz, E.C., Evans, S.M., Lee, S.K., and Pfaff, S.L. (2006). T-Box transcription factor Tbx20 regulates a genetic program for cranial motor neuron cell body migration. Development *133*, 4945–4955.

Stil, A., and Drapeau, P. (2016). Neuronal labeling patterns in the spinal cord of adult transgenic zebrafish. Dev. Neurobiol. *76*, 642–660.

Strong, M.J., Volkening, K., Hammond, R., Yang, W., Strong, W., Leystra-Lantz, C., and Shoesmith, C. (2007). TDP43 is a human low molecular weight neurofilament (hNFL) mRNA-binding protein. Mol. Cell. Neurosci. *35*, 320–327.

Taylor, A.M., Blurton-Jones, M., Rhee, S.W., Cribbs, D.H., Cotman, C.W., and Jeon, N.L. (2005). A microfluidic culture platform for CNS axonal injury, regeneration and transport. Nat. Methods *2*, 599–605.

Taylor, J.P., Brown, R.H., Jr., and Cleveland, D.W. (2016). Decoding ALS: from genes to mechanism. Nature *539*, 197–206.

Telfer, W.R., Busta, A.S., Bonnemann, C.G., Feldman, E.L., and Dowling, J.J. (2010). Zebrafish models of collagen VI-related myopathies. Hum. Mol. Genet. *19*, 2433–2444.

Tian, F., Yang, W., Mordes, D.A., Wang, J.Y., Salameh, J.S., Mok, J., Chew, J., Sharma, A., Leno-Duran, E., Suzuki-Uematsu, S., et al. (2016). Monitoring peripheral nerve degeneration in ALS by label-free stimulated Raman scattering imaging. Nat. Commun. *7*, 13283.

Tollervey, J.R., Curk, T., Rogelj, B., Briese, M., Cereda, M., Kayikci, M., Konig, J., Hortobagyi, T., Nishimura, A.L., Zupunski, V., et al. (2011). Characterizing the RNA targets and position-dependent splicing regulation by TDP-43. Nat. Neurosci. *14*, 452–458.

Wijesekera, L.C., and Leigh, P.N. (2009). Amyotrophic lateral sclerosis. Orphanet J. Rare Dis. *4*, 3.